Jiang, Cheng; Liu, Yu Long; Sillanpää, Mika A.

Energy-level attraction and heating-resistant cooling of mechanical resonators with exceptional points

Published in:
Physical Review A

DOI:
10.1103/PhysRevA.104.013502

Published: 01/06/2021

Document Version
Publisher's PDF, also known as Version of record

Please cite the original version:
Jiang, C., Liu, Y. L., & Sillanpää, M. A. (2021). Energy-level attraction and heating-resistant cooling of mechanical resonators with exceptional points. *Physical Review A*, *104*(1), Article 013502. https://doi.org/10.1103/PhysRevA.104.013502

Energy-level attraction and heating-resistant cooling of mechanical resonators with exceptional points

Cheng Jiang,[1,2] Yu-Long Liu ,[3,2,*] and Mika A. Sillanpää[2]
[1]*School of Physics and Electronic Electrical Engineering, Huaiyin Normal University, Huai'an 223300, China*
[2]*Department of Applied Physics, Aalto University, P.O. Box 15100, FI-00076 Aalto, Finland*
[3]*Beijing Academy of Quantum Information Sciences, Beijing 100193, China*

(Received 29 November 2020; accepted 21 June 2021; published 2 July 2021)

We study the energy-level evolution and ground-state cooling of mechanical resonators under a synthetic phononic gauge field. The tunable gauge phase is mediated by the phase difference between the $\mathcal{PT}$- and anti-$\mathcal{PT}$-symmetric mechanical couplings in a multimode optomechanical system. The transmission spectrum then exhibits an asymmetric Fano line shape or a double optomechanically induced transparency by modulating the gauge phase. Moreover, the eigenvalues will collapse and become degenerate, although the mechanical coupling is continuously increased. Such counterintuitive energy-level attraction, instead of anticrossing, is attributed to destructive interferences between $\mathcal{PT}$- and anti-$\mathcal{PT}$-symmetric couplings. We find that the energy-level attraction, as well as the accompanying exceptional points (EPs), can be clearly observed in the cavity output power spectrum where the mechanical eigenvalues correspond to distinct peaks. For mechanical cooling, the average phonon occupation number is minimized at the EPs. Especially, phonon transport becomes nonreciprocal and even ideally unidirectional at the EPs. Finally, we propose a heating-resistant ground-state cooling based on the nonreciprocal phonon transport, which is mediated by the gauge field. Towards the quantum regime of macroscopic mechanical resonators, most optomechanical systems are ultimately limited by their intrinsic cavity or mechanical heating. Our work shows that the thermal energy transfer can be blocked by tuning the gauge phase, which suggests a promising route to bypass the heating limitations.

DOI: 10.1103/PhysRevA.104.013502

I. INTRODUCTION

Non-Hermitian systems with parity-time ($\mathcal{PT}$) symmetry have attracted considerable attention since the pioneering work of Bender and Boettcher in 1998 [1]. The $\mathcal{PT}$-symmetric Hamiltonian H, which satisfies the commutation relation $[H, \hat{P}\hat{T}] = 0$ with the $\mathcal{PT}$ operator $\hat{P}\hat{T}$, can exhibit entirely real spectra under a specific parameter range. Moreover, an abrupt phase transition between the unbroken and broken symmetry occurs at the exceptional point (EP), where the eigenvalues and the corresponding eigenvectors coalesce. Experimental demonstrations of the $\mathcal{PT}$ symmetry and EP have revealed many intriguing phenomena such as unidirectional transmission [2,3], single-mode lasing [4,5], and enhanced sensitivity [6,7]. More comprehensive development related to $\mathcal{PT}$ symmetry can be found in Refs. [8–13].

On the other hand, the anti-$\mathcal{PT}$-symmetric Hamiltonian of growing interest satisfies $\{H, \hat{P}\hat{T}\} = 0$ and can possess purely imaginary eigenvalues. Recently, anti-$\mathcal{PT}$ symmetry has been widely observed in atomic systems [14,15], electrical circuits [16], diffusive thermal materials [17], a magnon-cavity-magnon coupled system [18], coupled waveguide systems [19,20], and a single microcavity with nonlinear Brillouin scattering [21]. Such systems can also display some noteworthy effects, including constant refraction [22], nonreciprocity and enhanced sensing [23], and information flow [24]. Compared with $\mathcal{PT}$-symmetric systems, anti-$\mathcal{PT}$-symmetric systems do not require any gain medium that may introduce extra instability and experimental complexity [25].

Optomechanical systems, which consist of an electromagnetic cavity coupled with a mechanical resonator via radiation pressure [26–28], have witnessed significant developments, such as ground-state cooling of the mechanical resonator [29–34], optomechanically induced transparency [35,36], and nonclassical states of motion [37,38]. More recently, multimode optomechanical systems comprising two or more mechanical resonators have been under intensive investigation [39–51]. The displacement of one mechanical resonator changes the cavity resonance and hence the intracavity photon number, which will, in turn, modify the radiation pressure on the other mechanical resonator [52–61]. For example, the mechanical resonators can be coupled through stimulated Raman adiabatic passage (STIRAP) [62–64]. These systems provide a platform to study synchronization [41,42] and entanglement [43,44] of the mechanical resonators, topological energy transfer [48], nonreciprocal phonon transport [50,51], and so on.

Furthermore, if the mechanical resonators are coupled directly through Coulomb interaction [65–67], a piezoelectric transducer [68], or a superconducting charge qubit [69], the multimode optomechanical system with loop interaction can exhibit exciting features such as nonreciprocal ground-state

*liuyl@baqis.ac.cn

cooling [59] and an enhanced second-order sideband [69]. Mechanical $\mathcal{PT}$ symmetry has also been demonstrated in two coupled optomechanical systems with the cavities being driven by blue- and red-detuned laser fields, respectively [70]. In these works, it is notable that the direct couplings between mechanical modes are coherent and $\mathcal{PT}$ symmetric. Energy localization and ground-state cooling at room temperature induced by broken $\mathcal{PT}$ symmetry have been proposed and discussed in detail in Refs. [71,72].

On the other hand, how anti-$\mathcal{PT}$ symmetry affects the mechanical cooling is intriguing but less discussed. In this paper, we study cooling of mechanical resonators in a multimode optomechanical system, which consists of two directly coupled mechanical resonators interacting with a common cavity field. Cooling of degenerate mechanical modes with a cavity-mediated mechanical dark-mode effect was discussed in Ref. [59]. We will focus on the nondegenerate case and study the optimal cooling under the conditions where the dark mode does not appear. When the cavity is red sideband driven at the average frequency of the two mechanical resonators, we derive the effective Hamiltonian for the mechanical modes by adiabatically eliminating the cavity field and find that mechanical anti-$\mathcal{PT}$ symmetry can be realized. Especially, when taking both the $\mathcal{PT}$- and anti-$\mathcal{PT}$-symmetric mechanical couplings into the consideration, a phononic gauge field with a tunable phase is synthesized. The EPs at which both the real and imaginary parts of the eigenvalues coalesce periodically appear at the phase-match points. The positions of the EPs can be shifted by modifying the relative strength between $\mathcal{PT}$- and anti-$\mathcal{PT}$-symmetric couplings, which in turn affects the phonon flow and the final phonon occupation numbers. Exploring how the phononic gauge field affects the energy-level evolution and the mechanical cooling are the main points of this article.

This paper is organized as follows. In Sec. II, we describe the multimode optomechanical system and then reveal anti-$\mathcal{PT}$-symmetric mechanical couplings mediated by a common cavity field. A phononic gauge field is subsequently constructed, and the periodic EPs are also presented in this section. In Sec. III, we demonstrate how to observe counterintuitive energy-level attraction around the EPs through the transmission and output spectra of the cavity. Then, the gauge-phase-controlled nonreciprocal phonon transport and heating-resistant cooling of the mechanical resonators are presented in Sec. IV. Finally, the conclusion of this paper is given in Sec. VI.

II. PHONONIC GAUGE FIELD AND EXCEPTIONAL POINTS

As shown in Fig. 1(a), the system consists of two mechanical resonators optomechanically coupled to a common cavity field. In addition, the two mechanical resonators are coupled with each other via phase-dependent phonon-exchange interaction which has been realized through the STIRAP of an auxiliary cavity mode [62–64]. The equivalent model is presented in Fig. 1(b), and the Hamiltonian of the system is

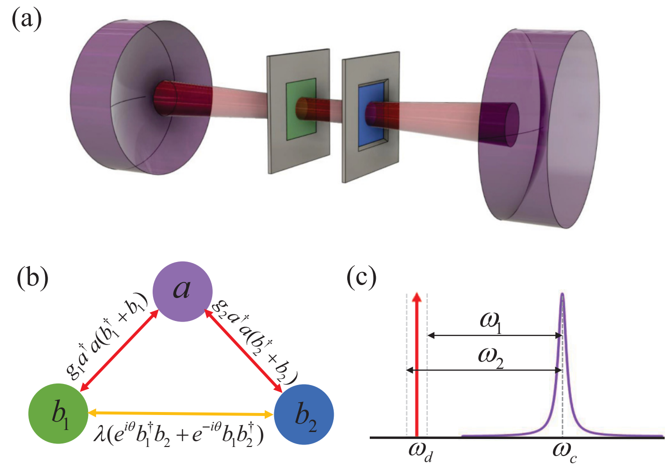

FIG. 1. (a) The multimode optomechanical system includes the cavity mode a and two mechanical modes $b_{1,2}$. Green and blue membranes represent mechanical modes b_1 and b_2, respectively. (b) Equivalent schematic diagram of the optomechanical mechanical system consisting of one cavity mode, a, and two mechanical modes, b_1 and b_2. The optical mode and the mechanical modes are coupled via radiation pressure, and the two mechanical modes are coupled directly with a phase-dependent coupling strength. (c) The driving scheme in the frequency domain. ω_c is the frequency of the cavity mode, ω_1 and ω_2 are the frequencies of the two mechanical modes, and ω_d is the frequency of the driving field, which is red detuned with respect to the cavity field by the average frequency of the two mechanical modes.

then given by

$$
\begin{aligned}
H =& \hbar\omega_c a^\dagger a + \sum_{k=1,2}\hbar\omega_k b_k^\dagger b_k + \sum_{k=1,2}\hbar g_k a^\dagger a(b_k^\dagger + b_k) \\
&+ \hbar\lambda(e^{i\theta}b_1^\dagger b_2 + e^{-i\theta}b_1 b_2^\dagger) + i\hbar\sqrt{\kappa_e}\varepsilon_d(a^\dagger e^{-i\omega_d t} - a e^{i\omega_d t}),
\end{aligned}
\tag{1}
$$

where $a^\dagger$ (a) are the creation (annihilation) operators of the cavity field with resonance frequency ω_c and $b_k^\dagger$ (b_k) are the creation (annihilation) operators of the mechanical resonators with resonance frequencies ω_k $(k = 1, 2)$. g_k is the single-photon optomechanical strength between the kth mechanical resonator and the cavity field. λ represents the coupling strength between the two mechanical resonators with the phase θ.

The last term in Eq. (1) describes the coupling between the driving field at frequency ω_d and the cavity field, where κ_e is the decay rate of the cavity due to external coupling and ε_d is the amplitude of the driving field. In the rotating frame at the driving frequency ω_d, the Hamiltonian becomes

$$
\begin{aligned}
H =& \hbar\Delta_c a^\dagger a + \sum_{k=1,2}\hbar\omega_k b_k^\dagger b_k + \sum_{k=1,2}\hbar g_k a^\dagger a(b_k^\dagger + b_k) \\
&+ \hbar\lambda(e^{i\theta}b_1^\dagger b_2 + e^{-i\theta}b_1 b_2^\dagger) + i\hbar\sqrt{\kappa_e}\varepsilon_d(a^\dagger - a),
\end{aligned}
\tag{2}
$$

where $\Delta_c = \omega_c - \omega_d$ is the detuning between the cavity and the driving field.

The dynamics of the system is determined by the following quantum Langevin equations:

$$\dot{a} = -\left(\frac{\kappa}{2}+i\Delta_c\right)a - ig_1(b_1^\dagger + b_1)a - ig_2(b_2^\dagger + b_2)a + \sqrt{\kappa_e}\varepsilon_L + \sqrt{\kappa_e}a_{\text{in},e} + \sqrt{\kappa_i}a_{\text{in},i}, \quad (3)$$

$$\dot{b_1} = -\left(\frac{\gamma_1}{2}+i\omega_1\right)b_1 - i\lambda e^{i\theta}b_2 - ig_1a^\dagger a + \sqrt{\gamma_1}b_{1,\text{in}}, \quad (4)$$

$$\dot{b_2} = -\left(\frac{\gamma_2}{2}+i\omega_2\right)b_2 - i\lambda e^{-i\theta}b_1 - ig_2a^\dagger a + \sqrt{\gamma_2}b_{2,\text{in}}, \quad (5)$$

where the total decay rate of the cavity $\kappa = \kappa_i + \kappa_e$ includes the intrinsic decay rate κ_i and the external decay rate κ_e because of the coupling to the feed line and γ_k is the damping rate of the kth mechanical resonator. a_{in} and $b_{k,\text{in}}$ represent the input quantum noise of the cavity and mechanical modes with zero mean values.

The steady-state solutions to Eqs. (3)–(5) can be obtained by setting the time derivatives to be zero, which are given by

$$\alpha = \frac{\sqrt{\kappa_e}\varepsilon_L}{\frac{\kappa}{2}+i\Delta},$$
$$\beta_1 = -\frac{ig_1(\gamma_2/2+i\omega_2)+\lambda e^{i\theta}g_2}{(\gamma_1/2+i\omega_1)(\gamma_2/2+i\omega_2)+\lambda^2}|\alpha|^2,$$
$$\beta_2 = -\frac{ig_2(\gamma_1/2+i\omega_1)+\lambda e^{-i\theta}g_1}{(\gamma_1/2+i\omega_1)(\gamma_2/2+i\omega_2)+\lambda^2}|\alpha|^2, \quad (6)$$

where $\Delta = \Delta_c + g_1(\beta_1^* + \beta_1) + g_2(\beta_2^* + \beta_2)$ is the effective cavity-driving field detuning including the radiation pressure effects. Equations (3)–(5) can be linearized by writing each operator as the sum of its steady-state solution and a small fluctuation, i.e., $a = \alpha + \delta a$, $b_1 = \beta_1 + \delta b_1$, and $b_2 = \beta_2 + \delta b_2$. Subsequently, we have

$$\delta\dot{a} = -\left(\frac{\kappa}{2}+i\Delta\right) - iG_1(\delta b_1^\dagger + \delta b_1) - iG_2(\delta b_2^\dagger + \delta b_2) + \sqrt{\kappa_e}a_{\text{in},e} + \sqrt{\kappa_i}a_{\text{in},i}, \quad (7)$$

$$\delta\dot{b_1} = -\left(\frac{\gamma_1}{2}+i\omega_1\right)\delta b_1 - i\lambda e^{i\theta}\delta b_2 - i(G_1^*\delta a + G_1\delta a^\dagger) + \sqrt{\gamma_1}b_{1,\text{in}}, \quad (8)$$

$$\delta\dot{b_2} = -\left(\frac{\gamma_2}{2}+i\omega_2\right)\delta b_2 - i\lambda e^{-i\theta}\delta b_1 - i(G_2^*\delta a + G_2\delta a^\dagger) + \sqrt{\gamma_2}b_{2,\text{in}}, \quad (9)$$

where $G_1 = g_1\alpha$ and $G_2 = g_2\alpha$ are the effective optomechanical coupling strengths.

In this work, we mainly consider the case in which the cavity is driven nearly on the red sideband of the mechanical resonators, i.e., $\Delta \approx \omega_m = (\omega_1 + \omega_2)/2$. The pump scheme is shown in Fig. 1(c). Equations (7)–(9) can be moved into another interaction picture by introducing the slowly moving operators with tildes, i.e., $\delta a = \delta\tilde{a}e^{-i\Delta t}$, $\delta b_1 = \delta\tilde{b_1}e^{-i\omega_m t}$, and $\delta b_2 = \delta\tilde{b_2}e^{-i\omega_m t}$. In the limit of $\omega_m \gg (G_{1,2}, \kappa)$, the rotating wave approximation can be invoked, and we can obtain the following equations:

$$\dot{a} = -\frac{\kappa}{2}a - iG_1b_1e^{-i\Delta_m t} - iG_2b_2e^{-i\Delta_m t} + \sqrt{\kappa_e}a_{\text{in},e} + \sqrt{\kappa_i}a_{\text{in},i}, \quad (10)$$

$$\dot{b_1} = -\left(\frac{\gamma_1}{2}+i\Omega\right)b_1 - i\lambda e^{i\theta}b_2 - iG_1^*ae^{i\Delta_m t} + \sqrt{\gamma_1}b_{1,\text{in}}, \quad (11)$$

$$\dot{b_2} = -\left(\frac{\gamma_2}{2}-i\Omega\right)b_2 - i\lambda e^{-i\theta}b_1 - iG_2^*ae^{i\Delta_m t} + \sqrt{\gamma_2}b_{2,\text{in}}, \quad (12)$$

where $\Delta_m = \omega_m - \Delta$, $\Omega = (\omega_1 - \omega_2)/2$, and we have replaced the symbol $\delta\tilde{o}$ ($o = a, b_1, b_2$) with o for simplicity. If $\Delta_m = 0$, the linearized Hamiltonian of the system is given by

$$H_L = \hbar\Omega b_1^\dagger b_1 - \hbar\Omega b_2^\dagger b_2 + \hbar\lambda(e^{i\theta}b_1^\dagger b_2 + e^{-i\theta}b_1b_2^\dagger) + \hbar(G_1a^\dagger b_1 + G_1^*ab_1^\dagger) + \hbar(G_2a^\dagger b_2 + G_2^*ab_2^\dagger). \quad (13)$$

Without loss of generality, we assume that the optomechanical coupling strengths G_1 and G_2 are positive real numbers. The phase θ can be viewed as a gauge phase in the loop formed by the cavity and mechanical modes (see details in Appendix A).

When the condition $\kappa \gg (G_{1,2}, \gamma_{1,2})$ is satisfied, the cavity field in Eqs. (10)–(12) can be adiabatically eliminated (see Appendix B), and we obtain the effective Hamiltonian for the two mechanical resonators

$$H_{\text{eff}}/\hbar = \begin{pmatrix} \Omega - i\left(\frac{\gamma}{2}+\Gamma\right) & \lambda e^{i\theta} - i\Gamma \\ \lambda e^{-i\theta} - i\Gamma & -\Omega - i\left(\frac{\gamma}{2}+\Gamma\right) \end{pmatrix}, \quad (14)$$

where we have assumed that $\Delta_m = 0$, $\gamma_1 = \gamma_2 = \gamma$, and $\Gamma = 2G^2/\kappa$. Hereafter, G_1 and G_2 are set to be equal, i.e., $G_1 = G_2 = G$. The eigenvalues of the Hamiltonian (14) are given by

$$\omega_\pm = -i\left(\frac{\gamma}{2}+\Gamma\right) \pm \sqrt{\Omega^2 + \lambda^2 - \Gamma^2 - 2i\Gamma\lambda\cos\theta}, \quad (15)$$

where the real parts of $\omega_\pm$ correspond to the resonance frequency of the mechanical eigenmodes and the imaginary parts represent their damping rates. If $\lambda = 0$, it is easy to check that non-Hermitian Hamiltonian (14) is anti-$\mathcal{PT}$ symmetric with an exceptional point at $\Gamma = \Omega$, which results from the dissipative coupling induced by the cavity.

In the presence of the direct coupling between the two mechanical resonators, the exceptional point is shifted to $\Gamma = \sqrt{\Omega^2 + \lambda^2}$ when $\theta = (2n+1)\pi/2$, with n being an integer. It is notable that the anti-$\mathcal{PT}$-symmetric coupling is a purely imaginary number with a fixed phase $\pi/2$, compared to the general $\mathcal{PT}$-symmetric coupling with a tunable phase θ here. Thus, the phase-match condition is satisfied when $\theta = (2n+1)(\pi/2)$, with $n \in \mathbb{Z}$. To demonstrate how the gauge field and phase affect the energy-level evaluation in this optomechanical system, we choose the experimentally realizable parameters from a recent work using microwave-frequency optomechanics [47]: $\omega_1/2\pi = 9.285$ MHz, $\omega_2/2\pi = 9.289$ MHz, $\gamma_1/2\pi = 100$ Hz, $\gamma_2/2\pi = 90$ Hz, $\kappa_e/2\pi = 410$ kHz, and $\kappa_i/2\pi = 268$ kHz. In Fig. 2, we plot the real and imaginary parts of the eigenvalues as functions of the (i) optomechanical coupling strength G and (ii) phase θ.

If two mechanical modes are not coupled directly ($\lambda = 0$), the solid lines in Figs. 2(a) and 2(b) show that the system can exhibit the anti-$\mathcal{PT}$ symmetry by modulating the coupling strength G. At lower values of G, the splitting between the two real parts of the eigenvalues is approximately equal to the

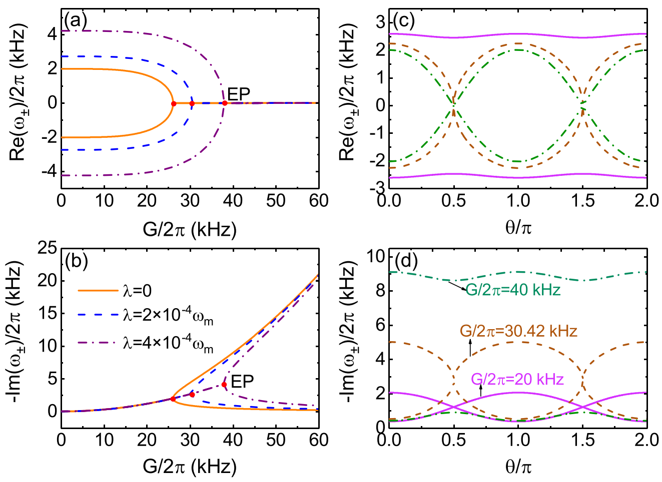

FIG. 2. (a) Real part $\mathrm{Re}[\omega_\pm]$ and (b) imaginary part $-\mathrm{Im}[\omega_\pm]$ of the eigenvalues as functions of the optomechanical coupling strength G with $\theta = \pi/2$ for different values of λ. (c) $\mathrm{Re}[\omega_\pm]$ and (d) $-\mathrm{Im}[\omega_\pm]$ versus the phase θ with $\lambda = 2\times 10^{-4}\omega_m$ for different values of G. The other parameters are $\omega_1/2\pi = 9.285$ MHz, $\omega_2/2\pi = 9.289$ MHz, $\gamma_1/2\pi = 100$ Hz, $\gamma_2/2\pi = 90$ Hz, $\kappa_e/2\pi = 410$ kHz, $\kappa_i/2\pi = 268$ kHz, $\omega_m = (\omega_1+\omega_2)/2$, and $\Delta = \omega_m$.

resonance frequency difference between the two mechanical modes, and the imaginary parts (damping rates) are nearly the same. With increasing the optomechanical coupling strength G, these two mechanical modes are coupled more strongly via their common interaction with the cavity field. However, the splitting between the two real parts $\mathrm{Re}(\omega_\pm)$ gets smaller; that is, the energy levels exhibit attraction. More specially, there exist EPs where both the real and imaginary parts of the eigenvalues coalesce. At higher values of G, the eigenvalues become purely imaginary, and the system resides in the unbroken anti-$\mathcal{PT}$-symmetric regime.

Such counterintuitive level attraction attributed to broken anti-$\mathcal{PT}$ symmetry differs from normal mode splitting observed with broken $\mathcal{PT}$ symmetry. As also shown in Fig. 2(a), if the two mechanical modes are coupled directly, the eigenvalues will be modified. When the coupling strength λ between the two mechanical modes is increased from 0 to $4\times 10^{-4}\omega_m$ with fixed phase $\theta = \pi/2$, the splitting between the two real parts $\mathrm{Re}(\omega_\pm)$ becomes larger, and the EP (red dot) is shifted to a higher value of G.

The phase dependence of the eigenvalues is plotted in Figs. 2(c) and 2(d). The splitting between the two real (imaginary) parts of the eigenvalues reaches the maximum at $\theta = n\pi$ and the minimum at $\theta = (2n+1)\pi/2 (n \in \mathbb{Z})$, i.e., when phase math is satisfied. By increasing the optomechanical coupling strength $G/2\pi$ from 20 to 40 kHz, the splitting between the two real parts gets smaller, but the splitting between the two imaginary parts becomes larger. Especially, when $G/2\pi = 30.42$ kHz, both the real and imaginary parts coalesce at the phase-match points, e.g., $n = (0, 1)$, corresponding to $\theta = (0.5, 1.5)\pi$. The EP in Figs. 2(c) and 2(d) with $\theta = 0.5\pi$ corresponds to the EP with $\lambda = 2\times 10^{-4}\omega_m$ in Figs. 2(a) and 2(b). We emphasize that the counterintuitive energy-level attraction originates from the destructive interference between the $\mathcal{PT}$- and anti-$\mathcal{PT}$-symmetric coupling paths from the gauge field. Furthermore, the exceptional points periodically appear when phase match is satisfied.

Notice that energy-level attraction between the cavity and a mechanical mode appears in a standard optomechanical system under blue-sideband pumping. The vastly different dissipation rates for the mechanical and electromagnetic modes makes it hard to observe the phenomenon, but it was experimentally verified in a microwave optomechanical circuit [73]. However, when crossing the EP, parametric instability occurs in the attraction regime. In our proposal, the energy-level attraction is mediated by the dissipation-induced anti-$\mathcal{PT}$-symmetric coupling, and the whole system is always stable and thus allows us to study the effects such as improved cooling at the stable EPs.

III. OBSERVATIONS OF LEVEL ATTRACTION THROUGH TRANSMISSION AND OUTPUT SPECTRA

Based on the optomechanical interactions, the cavity field supports a versatile platform to observe the mechanical levels. We now study the transmission and output spectrum of the cavity in this section. We define the vectors $\mu = (a, b_1, b_2)^{\mathrm{T}}$ for the system operators and $\mu_{\mathrm{in}} = (a_{\mathrm{in},e}, a_{\mathrm{in},i}, b_{1,\mathrm{in}}, b_{2,\mathrm{in}})^{\mathrm{T}}$ for the input operators; then Eqs. (10)–(12) can be written in the matrix form

$$\dot{\mu} = -M\mu + L\mu_{\mathrm{in}}, \tag{16}$$

where the coefficient matrix

$$M = \begin{pmatrix} \kappa/2 & iG & iG \\ iG & \gamma_1/2 + i\Omega & i\lambda e^{i\theta} \\ iG & i\lambda e^{-i\theta} & \gamma_2/2 - i\Omega \end{pmatrix} \tag{17}$$

and

$$L = \begin{pmatrix} \sqrt{\kappa_e} & \sqrt{\kappa_i} & 0 & 0 \\ 0 & 0 & \sqrt{\gamma_1} & 0 \\ 0 & 0 & 0 & \sqrt{\gamma_2} \end{pmatrix}. \tag{18}$$

Introducing the Fourier transform

$$o(\omega) = \int_{-\infty}^{\infty} o(t) e^{i\omega t} dt,$$
$$o^\dagger(\omega) = \int_{-\infty}^{\infty} o^\dagger(t) e^{i\omega t} dt, \tag{19}$$

the solution to Eq. (16) is then given by

$$\mu(\omega) = (M - i\omega)^{-1} L \mu_{\mathrm{in}}(\omega). \tag{20}$$

According to the input-output relation

$$\mu_{\mathrm{out}}(\omega) = \mu_{\mathrm{in}}(\omega) - L^{\mathrm{T}}\mu(\omega), \tag{21}$$

with $\mu_{\mathrm{out}}(\omega) = (a_{\mathrm{out},e}, a_{\mathrm{out},i}, b_{1,\mathrm{out}}, b_{2,\mathrm{out}})^{\mathrm{T}}$ being the vector for the output operators [74], we can obtain $\mu_{\mathrm{out}}(\omega) = S(\omega)\mu_{\mathrm{in}}(\omega)$, with the transmission matrix

$$S(\omega) = I_{4\times 4} - L^{\mathrm{T}}(M - i\omega)^{-1} L. \tag{22}$$

It is easy to derive that

$$S_{11}(\omega) = 1 - \kappa_e(\Gamma_1\Gamma_2 + \lambda^2)/d(\omega), \tag{23}$$

$$S_{12}(\omega) = -\sqrt{\kappa_e\kappa_i}(\Gamma_1\Gamma_2 + \lambda^2)/d(\omega), \tag{24}$$

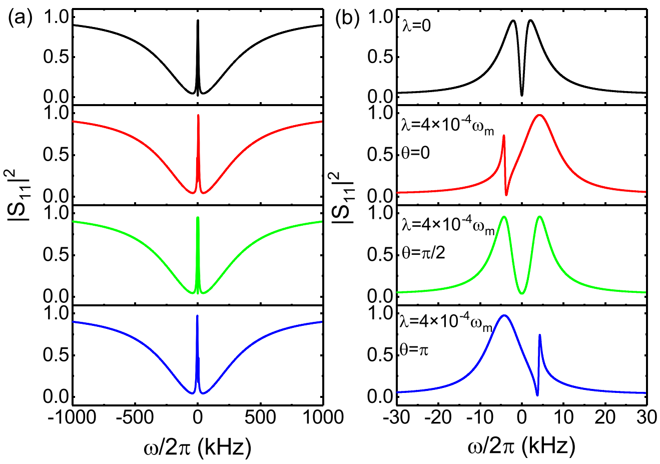

FIG. 3. (a) Transmission probability $|S_{11}|^2$ as a function of the probe detuning $\omega/2\pi$ for different values of the phase θ. (b) is a detail of (a) in the vicinity of $\omega = 0$. The other parameters are the same as those in Fig. 2 except $G/2\pi = 30$ kHz.

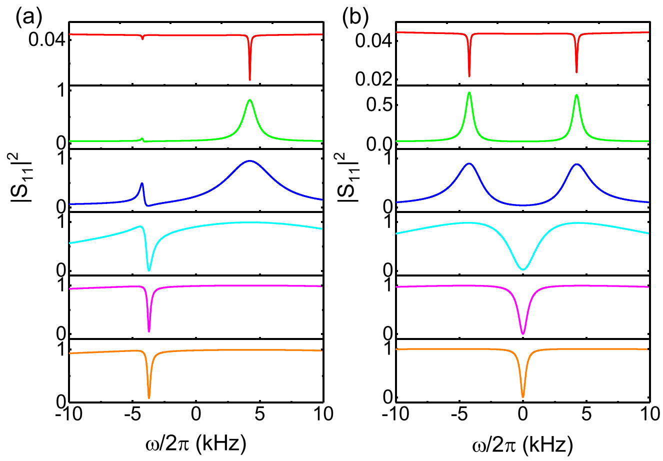

FIG. 4. Transmission probability $|S_{11}|^2$ as a function of the probe detuning $\omega/2\pi$ with (a) $\theta = 0$ and (b) $\theta = \pi/2$ for $G/2\pi = (1, 10, 20, 50, 90, 130)$ kHz from top to bottom. The other parameters are the same as those in Fig. 2 except $\lambda = 4 \times 10^{-4}\omega_m$.

$$S_{13}(\omega) = \sqrt{\kappa_e\gamma_1}G(i\Gamma_2 + \lambda e^{-i\theta})/d(\omega), \tag{25}$$

$$S_{14}(\omega) = \sqrt{\kappa_e\gamma_2}G(i\Gamma_1 + \lambda e^{i\theta})/d(\omega), \tag{26}$$

where $d(\omega) = \Gamma_c\Gamma_1\Gamma_2 + G^2(\Gamma_1 + \Gamma_2) + \Gamma_c\lambda^2 - 2i\lambda G^2\cos\theta$, with $\Gamma_c = \frac{\kappa}{2} - i\omega$, $\Gamma_1 = \frac{\gamma_1}{2} + i(\Omega - \omega)$, and $\Gamma_2 = \frac{\gamma_2}{2} - i(\Omega + \omega)$. The input quantum noises of the cavity and mechanical modes satisfy the correlation function

$$\langle a_{\text{in}}(\omega)a_{\text{in}}^\dagger(\omega')\rangle = 2\pi\delta(\omega + \omega'), \tag{27}$$

$$\langle b_{k,\text{in}}(\omega)b_{k,\text{in}}^\dagger(\omega')\rangle = 2\pi(n_k + 1)\delta(\omega + \omega'), \tag{28}$$

$$\langle b_{k,\text{in}}^\dagger(\omega)b_{k,\text{in}}(\omega')\rangle = 2\pi n_k\delta(\omega + \omega'), \tag{29}$$

where $n_k = 1/[\exp(\hbar\omega_k/k_B T_e) - 1]$ corresponds to the thermal phonon occupation of the mechanical mode at the environment temperature T_e. Recalling the input-output relations given in Eq. (21), the output spectrum of the cavity is given by

$$\begin{aligned} S_{\text{out}}(\omega) &= \frac{1}{2}\int \frac{d\omega'}{2\pi}\langle a_{\text{out},e}(\omega)a_{\text{out},e}^\dagger(\omega') + a_{\text{out},e}^\dagger(\omega')a_{\text{out},e}(\omega)\rangle \\ &= \frac{1}{2}|S_{11}(\omega)|^2 + \frac{1}{2}|S_{12}(\omega)|^2 + \left(n_1 + \frac{1}{2}\right)|S_{13}(\omega)|^2 \\ &\quad + \left(n_2 + \frac{1}{2}\right)|S_{14}(\omega)|^2. \end{aligned} \tag{30}$$

In Fig. 3, the transmission probability $|S_{11}|^2$ is plotted versus the probe detuning $\omega/2\pi$ when the phase θ varies. Figure 3(a) shows the transmission probability $|S_{11}|^2$ in a wide range of frequency, and the details of the peaks around $\omega = 0$ can be clearly seen from Fig. 3(b). If considering only the anti-$\mathcal{PT}$-symmetric coupling between the two mechanical modes (i.e., $\lambda = 0$), two symmetric transparency peaks locate at $\omega = \pm\Omega$, which can be referred to as double optomechanically induced transparency and explained by the interference effect [46,47]. When the two mechanical modes are coupled directly, the system forms a closed interaction loop, and the phase becomes important. If $\lambda = 4 \times 10^{-4}\omega_m$ and $\theta = \pi/2$, the two transparency windows are still symmetric, but the splitting between the two peaks is broadened. The positions of the peaks are approximately determined by $\omega = \pm\sqrt{\Omega^2 + \lambda^2}$ at low values of G, as shown in Fig. 2(a). However, if the phase θ is tuned to be zero or π, the transmission spectrum exhibits an asymmetric Fano line shape with a narrow dip and a broad transparency window induced by interference. Under the phononic gauge field, it is notable that symmetric transparency exists only in the case of phase matching. The other way around, the position of the transmission dip can be controlled by the phase θ; however, the analytical expression is too cumbersome to present here. When the power of the driving field is increased, the effective optomechanical coupling strength will be enhanced. Figure 4 plots the transmission probability $|S_{11}|^2$ as a function of the probe detuning $\omega/2\pi$ for a number of G values with $\theta = 0$ [Fig. 4(a)] and $\theta = \pi/2$ [Fig. 4(b)]. At $G/2\pi = 1$ kHz, the anti-$\mathcal{PT}$-symmetric coupling between the two mechanical modes mediated by the radiation pressure is weak, and the transmission spectrum exhibits two narrow dips around the cavity center due to the anti-Stokes scattering process. When the optomechanical coupling strength is enhanced to $G/2\pi = 10$ kHz, the two dips turn into two peaks, which results from the destructive interference between the anti-Stokes field and the probe field. Note that the two peaks are asymmetric at $\theta = 0$ but symmetric at $\theta = \pi/2$ (i.e., phase matched with $n = 0$).

With further increasing the coupling strength G, the linewidth of the peaks is broadened. Under phase matching, e.g., $\theta = \pi/2$, the linewidth is given by the effective mechanical damping rate $\gamma_{k,\text{eff}} = \gamma_k + \gamma_{k,\text{opt}}$, with $\gamma_{k,\text{opt}} = 4G_k^2/\kappa$. When the condition $\gamma_{k,\text{eff}} > |\omega_1 - \omega_2|$ is satisfied [47] around the EP, the individual mechanical modes have a large spectral overlap, and the two transmission peaks gradually merge into a single dip in the cavity center. The linewidth of the transmission dip becomes smaller with the increase of the coupling strength G, which is also seen from the lower branch of the curve above the EP in Fig. 2(b). At $\theta = 0$, the transmission

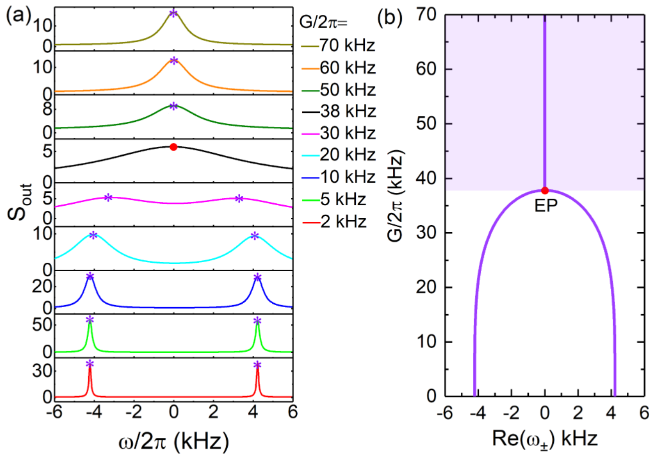

FIG. 5. (a) Cavity output spectrum versus the probe detuning $\omega/2\pi$ for varying optomechanical coupling strength from $G/2\pi = 2$ kHz (bottom curve) to $G/2\pi = 70$ kHz (top curve). The asterisks mark the mechanical levels. (b) The real part $\mathrm{Re}[\omega_\pm]$ of the eigenvalue versus the coupling strength $G/2\pi$. The other parameters are the same as those in Fig. 4 except $n_1 = n_2 = 100$ and $\theta = \pi/2$. Red dots mark the EP under the phase match.

dip is evolved from the asymmetric Fano line shape with zero transmission probability on the left of Fig. 4(a). Figure 4 clearly shows that mechanical level attraction occurs when the phase-match condition is satisfied.

Furthermore, the exceptional point in this optomechanical system is even more evident in the cavity output spectrum. As shown in Fig. 5, at low values of the optomechanical coupling strength G, two symmetric peaks can be observed in the output spectrum, which corresponds to the two mechanical eigenmodes. When the strength $G/2\pi$ is increased from 2 to 30 kHz, the splitting between the two peaks becomes smaller, but the linewidth gets larger. At $G/2\pi = 38$ kHz, i.e., the exceptional point, the two peaks merge into a single peak in the cavity center, which represents the level attraction between two mechanical modes. The position of the single peak remains the same, but the linewidth decreases with further increasing the coupling strength G. In particular, the envelope of the peak values in Fig. 5(a) forms the curve for the real part $\mathrm{Re}(\omega_\pm)$ of the eigenvalues shown in Fig. 5(b).

IV. IMPROVED COOLING AT THE EXCEPTIONAL POINTS

Taking dissipation into consideration, the evolution of the density matrix of the optomechanical system is governed by the quantum master equation

$$\dot{\rho} = -\frac{i}{\hbar}[H_L, \rho] + \kappa\mathcal{D}[a]\rho + \gamma_1(n_1+1)\mathcal{D}[b_1]\rho + \gamma_1 n_1\mathcal{D}[b_1^\dagger]\rho + \gamma_2(n_2+1)\mathcal{D}[b_2]\rho + \gamma_2 n_2\mathcal{D}[b_2^\dagger]\rho, \quad (31)$$

where $\mathcal{D}[o]\rho = o\rho o^\dagger - \frac{1}{2}o^\dagger o\rho - \frac{1}{2}\rho o^\dagger o$ is the standard Lindblad superoperator for the dissipations of the cavity and mechanical modes and the Hamiltonian H_L is given by Eq. (13). According to $\langle\dot{o}\rangle = \mathrm{Tr}\{o\dot{\rho}\}$, we can obtain the time evolution of the second-order moments, $\langle a^\dagger a\rangle$, $\bar{n}_1 = \langle b_1^\dagger b_1\rangle$, $\bar{n}_2 = \langle b_2^\dagger b_2\rangle$, $\langle a^\dagger b_1\rangle$, $\langle a^\dagger b_2\rangle$, and $\langle b_1^\dagger b_2\rangle$. The differential equations are given by

$$\frac{d}{dt}\langle a^\dagger a\rangle = -\kappa\langle a^\dagger a\rangle - iG(\langle a^\dagger b_1\rangle + \langle a^\dagger b_2\rangle - \langle a^\dagger b_1\rangle^* - \langle a^\dagger b_2\rangle^*), \quad (32)$$

$$\frac{d}{dt}\langle b_1^\dagger b_1\rangle = -\gamma_1\langle b_1^\dagger b_1\rangle + i(G\langle a^\dagger b_1\rangle - G\langle a^\dagger b_1\rangle^* - \lambda e^{i\theta}\langle b_1^\dagger b_2\rangle + \lambda e^{-i\theta}\langle b_1^\dagger b_2\rangle^*) + \gamma_1 n_1, \quad (33)$$

$$\frac{d}{dt}\langle b_2^\dagger b_2\rangle = -\gamma_2\langle b_2^\dagger b_2\rangle + i(G\langle a^\dagger b_2\rangle - G\langle a^\dagger b_2\rangle^* + \lambda e^{i\theta}\langle b_1^\dagger b_2\rangle - \lambda e^{-i\theta}\langle b_1^\dagger b_2\rangle^*) + \gamma_2 n_2, \quad (34)$$

$$\frac{d}{dt}\langle a^\dagger b_1\rangle = \left(-\frac{\kappa+\gamma_1}{2} - i\Omega\right)\langle a^\dagger b_1\rangle + i(G\langle b_1^\dagger b_1\rangle + G\langle b_1^\dagger b_2\rangle^* - G\langle a^\dagger a\rangle - \lambda e^{i\theta}\langle a^\dagger b_2\rangle), \quad (35)$$

$$\frac{d}{dt}\langle a^\dagger b_2\rangle = \left(-\frac{\kappa+\gamma_2}{2} + i\Omega\right)\langle a^\dagger b_2\rangle + i(G\langle b_1^\dagger b_2\rangle + G\langle b_2^\dagger b_2\rangle - G\langle a^\dagger a\rangle - \lambda e^{-i\theta}\langle a^\dagger b_1\rangle), \quad (36)$$

$$\frac{d}{dt}\langle b_1^\dagger b_2\rangle = \left(-\frac{\gamma_1+\gamma_2}{2} + 2i\Omega\right)\langle b_1^\dagger b_2\rangle + i(G\langle a^\dagger b_2\rangle - G\langle a^\dagger b_1\rangle^* - \lambda e^{-i\theta}\langle b_1^\dagger b_1\rangle + \lambda e^{-i\theta}\langle b_2^\dagger b_2\rangle). \quad (37)$$

In the steady state, all the derivatives in Eqs. (32)–(37) equal to zero. Under the condition of $\kappa > G \gg \{\lambda, \Omega, \gamma_{1,2}\}$, with $\gamma_m = (\gamma_1+\gamma_2)/2$, the final average phonon numbers can be obtained as

$$\bar{n}_1^f \approx \frac{2(\Gamma^2-\lambda^2)\gamma_1 n_1 + 2(\Gamma\mp\lambda)^2\gamma_2 n_2}{[\gamma_m^2 + 4(\lambda^2+\Omega^2+\Gamma\gamma_m)](2\Gamma+\gamma_m)} + \frac{\gamma_1 n_1}{2\Gamma+\gamma_m}, \quad (38)$$

$$\bar{n}_2^f \approx \frac{2(\Gamma\pm\lambda)^2\gamma_1 n_1 + 2(\Gamma^2-\lambda^2)\gamma_2 n_2}{[\gamma_m^2 + 4(\lambda^2+\Omega^2+\Gamma\gamma_m)](2\Gamma+\gamma_m)} + \frac{\gamma_2 n_2}{2\Gamma+\gamma_m}, \quad (39)$$

where the upper (lower) sign in $\mp$ and $\pm$ corresponds to $\theta = \pi/2$ $(3\pi/2)$.

The first terms in Eqs. (38) and (39) are the added steady-state phonon numbers from cavity-mediated mechanical mode couplings. The second terms are the regular cooling limit for the standard resolved sideband cooling of a single mechanical mode by a cavity. Under phase matching and with balanced $\mathcal{PT}$ and anti-$\mathcal{PT}$ coupling strengths (i.e., at the EPs), the first terms could be zero, and the added steady-state phonon number arising from the other mechanical thermal bath and the dark-mode limitations could be totally canceled. Thus, the cooling limit again meets the single-mode limit.

We study the cooling of the mechanical resonators by numerically solving Eqs. (32)–(37). Figure 6(a) plots the time

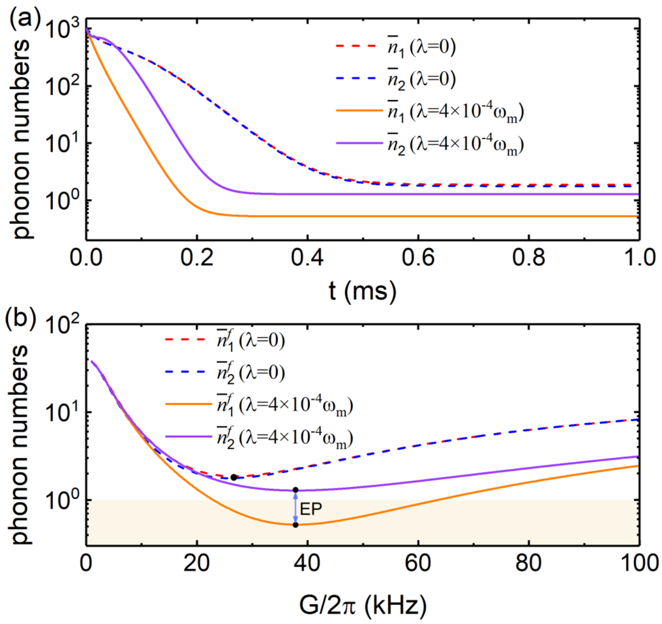

FIG. 6. (a) The time evolution of the average phonon numbers $\bar{n}_1$ and $\bar{n}_2$ when the mechanical-mechanical coupling is turned off ($\lambda = 0, G/2\pi = 26$ kHz, dashed lines) and on ($\lambda = 4 \times 10^{-4}\omega_m, \theta = \pi/2, G/2\pi = 38$ kHz, solid lines). (b) The final average phonon numbers $\bar{n}_1^f$ and $\bar{n}_2^f$ as a function of the optomechanical coupling strength $G/2\pi$ when $\lambda = 0$ (dashed lines) and $\lambda = 4 \times 10^{-4}\omega_m, \theta = \pi/2$ (solid lines). The black solid dots located at the minimum phonon number mark the EP. The other parameters are the same as those in Fig. 4 except $n_1 = n_2 = 40$.

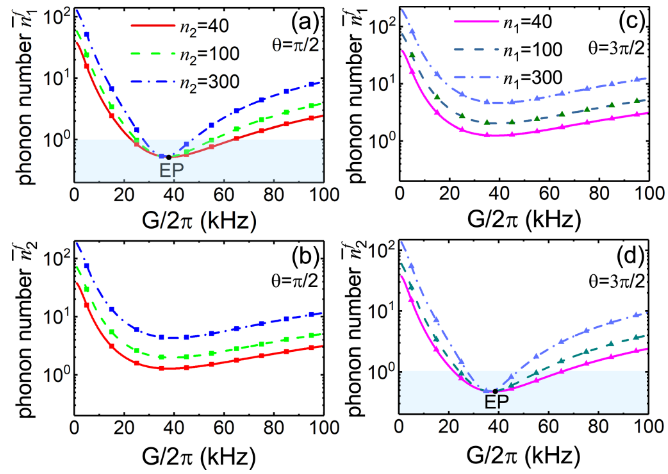

FIG. 7. The final average phonon numbers $\bar{n}_1^f$ and $\bar{n}_2^f$ versus the optomechanical coupling strength G for different thermal phonon occupations with (a) and (b) $\theta = \pi/2$ and (c) and (d) $\theta = 3\pi/2$. The curves and the symbols correspond to the numerical results based on Eqs. (32)–(37) and the analytical results of Eqs. (38) and (39), respectively. The other parameters are the same as those in Fig. 4 except $n_1 = 40$ in (a) and (b) and $n_2 = 40$ in (c) and (d).

evolution of the average phonon numbers without and with the $\mathcal{PT}$-symmetric direct coupling between the mechanical resonators. Without $\mathcal{PT}$-symmetric couplings, i.e., $\lambda = 0$, the final steady-state phonon occupations are almost the same for these two mechanical modes. For example, steady-state phonon numbers are $\bar{n}_1 \approx 1.9$ and $\bar{n}_2 \approx 1.8$, with $G/2\pi = 26$ kHz. Neither of these two mechanical modes reach the ground state if they just have optomechanically mediated anti-$\mathcal{PT}$-symmetric couplings.

The final (steady-state) average phonon numbers $\bar{n}_1^f$ and $\bar{n}_2^f$ versus the optomechanical coupling strength G are plotted in Fig. 6(b). At a further increase in G, the phonon numbers start to monotonically increase instead of further cooling as expected. Recall from the EP discussions [e.g., EPs in Fig. 2(a)] that the system undergoes a transition into the symmetry-broken phase where the dark modes formed by the mechanical modes decouple from the cavity mode and prevent us from extracting energy from the dark modes through the cooling channel of the cavity mode.

We now discuss how the phononic gauge field will affect mechanical cooling. As shown in Fig 6, the two mechanical resonators can be further cooled by turning on the $\mathcal{PT}$-symmetric direct coupling, i.e., by constructing a phononic gauge field. It is shown that $\bar{n}_1^f \approx 0.5$ and $\bar{n}_2^f \approx 1.3$ in the steady state at $\lambda = 4 \times 10^{-4}\omega_m$, $\theta = \pi/2$, and $G/2\pi = 38$ kHz. We emphasize that with such a phononic gauge field and under the phase matching (e.g., $n = 1$, $\theta = \pi/2$), (i) both mechanical resonators hold smaller steady-state phonon numbers, (ii) with the increase of the value G, the final average phonon numbers decrease monotonically and reach the minimum at the EP, and (iii) the final steady-state phonon occupations are quite different and the ground-state cooling for mode 1 is realized. By further increasing G until it crosses the EP, the final average phonon numbers starts to increase again. This breakdown of the cooling is attributed to the mechanical dark mode formed in the symmetry-broken regime.

From the above calculations, we find that (i) the optimal cooling with minimum phonon number occurs at the EP, (ii) the cooling is improved when the phase matching between $\mathcal{PT}$- and anti-$\mathcal{PT}$-symmetric couplings is taken into consideration, and (iii) the ground-state cooling is accessible for either of the mechanical modes. When n is an even (odd) number, mechanical mode b_2 (b_1) can be cooled down to its ground state. When modes are nearly degenerate, continuously increasing optomechanical coupling will introduce the mechanical dark mode [47]. Then, the mechanical modes start to decouple from the cavity field, and they cannot be further cooled down. The dark mode forms at the EPs. At a nonzero direct coupling, the EP appears at a higher value of G. Thus, a stronger G is allowed before the formation of the dark modes. Subsequently, the cooling limit is decreased.

Equations (38) and (39) also show that the thermal phonon energy transfer is unidirectional. The direction is dependent on the parity of n. In the following, we will discuss how the unidirectional phonon transfer can be used to protect the ground-state cooling from mechanical heating.

V. HEATING-RESISTANT GROUND-STATE COOLING

Finally, we discuss how the gauge phase affects the thermal phonon transport and the mechanical cooling performance. Figures 7(a) and 7(b) plot the final average phonon numbers $\bar{n}_1^f$ and $\bar{n}_2^f$ as a function of the coupling strength G with

$\theta = \pi/2$ (i.e., $n = 0$) and $n_1 = 40$ for different values of n_2. It is shown that both the final average phonon numbers $\bar{n}_1^f$ and $\bar{n}_2^f$ increase with the thermal phonon occupation n_2. However, the minimum value of $\bar{n}_1^f$ stays constant at the exceptional point when the thermal phonon occupation n_2 increases, which demonstrates the robustness of the cooling limit in the first mechanical resonator against thermal noise of the second mechanical resonator at the EP. It can also be seen from Eq. (38) that $\bar{n}_1^f$ is independent of n_2 when $\theta = \pi/2$ and $\Gamma = \lambda$, which is consistent with the numerical results. If the phase is tuned to be $\theta = 3\pi/2$ (i.e., $n = 1$), Fig. 7(d) shows that the second mechanical resonator can be cooled to the ground state at the EP, which is also robust against the thermal noise of the first mechanical resonator.

This phenomenon is closely related to the nonreciprocal phonon transfer which becomes ideally unidirectional at the EPs. Recalling Eqs. (38) and (39), we reveal that the thermal noise transport from mechanical mode 2 (1) to 1 (2) is blocked when n is an even (odd) number. We can thus conclude that thermal energy transfer can be controlled by tuning the gauge phase, which suggests a promising route to bypass unequal mechanical occupations due to, e.g., technical heating in the experiment. Note that for the resolved sideband regime ($\kappa < \omega_{1,2}$) under consideration, Stokes scattering due to the finite cavity linewidth limits the final average phonon number to $\bar{n}_{ba} = (\kappa/4\omega_m)^2 \approx 3 \times 10^{-4}$ [75,76], which can be neglected here.

VI. CONCLUSION

In summary, we have investigated energy-level evolution and cooling of mechanical resonators under a phase-tunable phononic gauge field. By adiabatically eliminating the cavity mode, we have shown that the effective coupling between two mechanical modes can be purely imaginary, which satisfies anti-$\mathcal{PT}$ symmetry. By considering another $\mathcal{PT}$-symmetric direct coupling, a phononic gauge field with tunable phase was constructed. The transmission spectrum then exhibited an asymmetric Fano line shape or double optomechanically induced transparency depending on the gauge phase. We then showed how a counterintuitive energy-level attraction accompanied by periodical EPs can be observed under phase matching. In addition to the transmission spectrum, we proposed that such energy-level attraction and the corresponding EPs are very evident in the cavity output power spectrum where the mechanical eigenvalues correspond to peaks.

The gauge field and its phase also greatly affect the phonon transport. Especially for mechanical cooling, the average phonon occupation number reaches the minimum at these EPs, and the mechanical resonator cools very close to the ground state. Moreover, destructive interference takes place within the gauge field, and then the phonon transport becomes nonreciprocal and even ideally unidirectional at the EPs under phase matching. The thermal blockade direction is switchable and controlled by the gauge phase. Finally, we proposed a heating-resistant ground-state cooling based on the nonreciprocal phonon transport. It can allow for mitigating intrinsic cavity or mechanical heating originating from material defects, photothermal conversion, or phase noise, which otherwise impose limitations on optomechanical experiments in the quantum regime of macroscopic mechanical resonators.

Moreover, the proposed gauge phase in this work provides a reconfigurable parameter for observing the Riemann sheet [10–13]. Our work may motivate more explorations towards heating-resistant cooling, utilizing, e.g., the topological protection arising from encircling the EPs [77,78].

ACKNOWLEDGMENTS

This work was supported by the Academy of Finland (Contracts No. 307757, No. 312057), by the European Research Council (Grant No. 615755), and by the Aalto Centre for Quantum Engineering. The work was performed as part of the Academy of Finland Centre of Excellence program (Project No. 336810). We acknowledge funding from the European Union's Horizon 2020 research and innovation program under Grant Agreement No. 732894 (FETPRO HOT). C.J. was supported by the Natural Science Foundation of China under Grant No. 11874170 and the Qinglan Project of Jiangsu Province of China. Y.-L.L. acknowledges the financial support from the Natural Science Foundation of China under Grant No. 12004044.

APPENDIX A: GAUGE PHASE

In Sec. II, we assumed that the optomechanical coupling strengths G_1 and G_2 are positive real numbers and θ represents a gauge phase. Here, we explain this assumption by redefining operators b_1 and b_2. In general, the coupling strengths $G_1 = g_1\alpha = |G_1|e^{i\theta_1}$ and $G_2 = g_2\alpha = |G_2|e^{i\theta_2}$, with $\theta_1 = \theta_2$. We redefine the operators as

$$b_1 \rightarrow b_1 e^{-i\theta_1}, \quad b_2 \rightarrow b_2 e^{-i\theta_2}; \tag{A1}$$

then the linearized Hamiltonian (13) becomes

$$\begin{aligned} H_L &= \hbar\Omega b_1^\dagger b_1 - \hbar\Omega b_2^\dagger b_2 \\ &\quad + \hbar\lambda[e^{i(\theta+\theta_1-\theta_2)} b_1^\dagger b_2 + e^{-i(\theta+\theta_1-\theta_2)} b_1 b_2^\dagger] \\ &\quad + \hbar(|G_1|a^\dagger b_1 + |G_1| a b_1^\dagger) + \hbar(|G_2|a^\dagger b_2 + a b_2^\dagger). \end{aligned} \tag{A2}$$

Therefore, by redefining the operators, the phase $\theta = \theta + \theta_1 - \theta_2$ can be treated as a gauge phase in the loop formed by modes a, b_1, b_2, and the coupling strengths $G_{1,2} \rightarrow |G_{1,2}|$ become positive real numbers.

APPENDIX B: ADIABATIC ELIMINATION

In order to obtain the effective Hamiltonian of the mechanical resonators, we neglect the noise terms for simplicity. According to Eq. (10), we can obtain the formal solution of a as

$$\begin{aligned} a(t) &= -iG_1 \int_0^t dt' b_1(t') e^{-i\Delta_m t'} e^{-\frac{\kappa}{2}(t-t')} \\ &\quad - iG_2 \int_0^t dt' b_2(t') e^{-i\Delta_m t'} e^{-\frac{\kappa}{2}(t-t')}. \end{aligned} \tag{B1}$$

If the decay rate of the cavity is large enough and satisfies $\kappa \gg \gamma_1, \gamma_2$, then changes in modes 1 and 2 are small within the integration range. Therefore, we can set $b_1(t') \approx b_1(t)$, $b_2(t') \approx b_2(t)$ and then take them out of the integral in

Eq. (B1) to obtain

$$\begin{aligned} a(t) &= -iG_1 b_1(t)\int_0^t dt' e^{-i\Delta_m t'} e^{-\frac{\kappa}{2}(t-t')} \\ &\quad - iG_2 b_2(t)\int_0^t dt' e^{-i\Delta_m t'} e^{-\frac{\kappa}{2}(t-t')} \\ &= -iG_1 b_1(t)\frac{e^{-i\Delta_m t}}{\frac{\kappa}{2}-i\Delta_m} - iG_2 b_2(t)\frac{e^{-i\Delta_m t}}{\frac{\kappa}{2}-i\Delta_m}. \end{aligned} \tag{B2}$$

Substituting Eq. (B2) into Eqs. (11) and (12), we can adiabatically eliminate the cavity mode a to obtain the following equations of motion for mechanical modes b_1 and b_2:

$$\dot{b_1} = -\left(\frac{\gamma_1}{2} + i\Omega + \frac{|G_1|^2}{\frac{\kappa}{2}-i\Delta_m}\right)b_1 - \left(\frac{G_1^* G_2}{\frac{\kappa}{2}-i\Delta_m} + i\lambda e^{i\theta}\right)b_2, \tag{B3}$$

$$\dot{b_2} = -\left(\frac{\gamma_2}{2} - i\Omega + \frac{|G_2|^2}{\frac{\kappa}{2}-i\Delta_m}\right)b_2 - \left(\frac{G_1 G_2^*}{\frac{\kappa}{2}-i\Delta_m} + i\lambda e^{-i\theta}\right)b_1. \tag{B4}$$

Equations (B3) and (B4) can be written in matrix form as

$$\begin{aligned} i\frac{d}{dt}\begin{pmatrix} b_1 \\ b_2 \end{pmatrix} \\ = \begin{pmatrix} \Omega - i\left(\frac{\gamma}{2} + \frac{|G_1|^2}{\kappa/2-i\Delta_m}\right) & \lambda e^{i\theta} - i\frac{G_1^* G_2}{\kappa/2-i\Delta_m} \\ \lambda e^{-i\theta} - i\frac{G_1 G_2^*}{\kappa/2-i\Delta_m} & -\Omega - i\left(\frac{\gamma_2}{2} + \frac{|G_2|^2}{\kappa/2-i\Delta_m}\right) \end{pmatrix}\begin{pmatrix} b_1 \\ b_2 \end{pmatrix}. \end{aligned} \tag{B5}$$

Therefore, the effective Hamiltonian for the two mechanical resonators is given by

$$H_{\rm eff}/\hbar = \begin{pmatrix} \Omega - i\left(\frac{\gamma_1}{2} + \frac{|G_1|^2}{\kappa/2-i\Delta_m}\right) & \lambda e^{i\theta} - i\frac{G_1^* G_2}{\kappa/2-i\Delta_m} \\ \lambda e^{-i\theta} - i\frac{G_1 G_2^*}{\kappa/2-i\Delta_m} & -\Omega - i\left(\frac{\gamma_2}{2} + \frac{|G_2|^2}{\kappa/2-i\Delta_m}\right) \end{pmatrix}. \tag{B6}$$

If the damping rates of the two mechanical resonators are equal ($\gamma_1 = \gamma_2 = \gamma$), the effective optomechanical coupling strengths are the same and real ($G_1 = G_2 = G$), and the cavity is driven close to the red sideband ($\Delta_m = 0$), the effective Hamiltonian (B6) is reduced to

$$H_{\rm eff}/\hbar = \begin{pmatrix} \Omega - i\left(\frac{\gamma}{2} + \Gamma\right) & \lambda e^{i\theta} - i\Gamma \\ \lambda e^{-i\theta} - i\Gamma & -\Omega - i\left(\frac{\gamma}{2} + \Gamma\right) \end{pmatrix}, \tag{B7}$$

where $\Gamma = 2G^2/\kappa$. Equivalently, the Hamiltonian (B7) can be written as

$$\begin{aligned} H_{\rm eff}/\hbar &= \left[\Omega - i\left(\frac{\gamma}{2} + \Gamma\right)\right]b_1^\dagger b_1 - \left[\Omega + i\left(\frac{\gamma}{2} + \Gamma\right)\right]b_2^\dagger b_2 \\ &\quad + (\lambda e^{-i\theta} - i\Gamma)b_1^\dagger b_2 + (\lambda e^{i\theta} - i\Gamma)b_1 b_2^\dagger. \end{aligned} \tag{B8}$$

We note that the coupling between the two mechanical resonators can be classified into two categories. The term $H_{I1} = \lambda e^{-i\theta} b_1^\dagger b_2 + \lambda e^{i\theta} b_1 b_2^\dagger$ represents the $\mathcal{PT}$-symmetric coupling since $(\mathcal{PT})H_{I1}(\mathcal{PT})^{-1} = H_{I1}$ under the parity $\mathcal{P}$ (i.e., $b_1 \leftrightarrow b_2$) and time-reversal $\mathcal{T}$ (i.e., $i \leftrightarrow -i$) operations. The term $H_{I2} = -i\Gamma b_1^\dagger b_2 - i\Gamma b_1 b_2^\dagger$ corresponds to the anti-$\mathcal{PT}$-symmetric coupling since $(\mathcal{PT})H_{I2}(\mathcal{PT})^{-1} = -H_{I2}$ under the parity $\mathcal{P}$ and time-reversal $\mathcal{T}$ operations.

[1] C. M. Bender and S. Boettcher, Real Spectra in Non-Hermitian Hamiltonians Having $\mathcal{PT}$ Symmetry, Phys. Rev. Lett. **80**, 5243 (1998).

[2] B. Peng, Ş. K. Özdemir, F. Lei, F. Monifi, M. Gianfreda, G. L. Long, S. Fan, F. Nori, C. M. Bender, and L. Yang, Parity-time-symmetric whispering-gallery microcavities, Nat. Phys. **10**, 394 (2014).

[3] L. Chang, X. Jiang, S. Hua, C. Yang, J. Wen, L. Jiang, G. Li, G. Wang, and M. Xiao, Parity-time symmetry and variable optical isolation in active-passive-coupled microresonators, Nat. Photonics **8**, 524 (2014).

[4] L. Feng, Z. J. Wong, R.-M. Ma, Y. Wang, and X. Zhang, Single-mode laser by parity-time symmetry breaking, Science **346**, 972 (2014).

[5] H. Hodaei, M.-A. Miri, M. Heinrich, D. N. Christodoulides, and M. Khajavikhan, Parity-time-symmetric microring lasers, Science **346**, 975 (2014).

[6] H. Hodaei, A. U. Hassan, S. Wittek, H. Garcia-Gracia, R. El-Ganainy, D. N. Christodoulides, and M. Khajavikhan, Enhanced sensitivity at higher-order exceptional points, Nature (London) **548**, 187 (2017).

[7] W. Chen, Ş. K. Özdemir, G. Zhao, J. Wiersig, and L. Yang, Exceptional points enhance sensing in an optical microcavity, Nature (London) **548**, 192 (2017).

[8] A. A. Zyablovsky, A. P. Vinogradov, A. A. Pukhov, A. V. Dorofeenko, and A. A. Lisyansky, PT-symmetry in optics, Phys. Usp. **57**, 1063 (2014).

[9] V. V. Konotop, J. Yang, and D. A. Zezyulin, Nonlinear waves in $\mathcal{PT}$-symmetric systems, Rev. Mod. Phys. **88**, 035002 (2016).

[10] L. Feng, R. El-Ganainy, and L. Ge, Non-Hermitian photonics based on parity-time symmetry, Nat. Photonics **11**, 752 (2017).

[11] R. El-Ganainy, K. G. Makris, M. Khajavikhan, Z. H. Musslimani, S. Rotter, and D. N. Christodoulides, Non-Hermitian physics and PT symmetry, Nat. Phys. **14**, 11 (2018).

[12] M.-A. Miri and A. Alù, Exceptional points in optics and photonics, Science **363**, eaar7709 (2019).

[13] Ş. K. Özdemir, S. Rotter, F. Nori, and L. Yang, Parity-time symmetry and exceptional points in photonics, Nat. Mater. **18**, 783 (2019).

[14] P. Peng, W. Cao, C. Shen, W. Qu, J. Wen, L. Jiang, and Y. Xiao, Anti-parity-time symmetry with flying atoms, Nat. Phys. **12**, 1139 (2016).

[15] Y. Jiang, Y. Mei, Y. Zuo, Y. Zhai, J. Li, J. Wen, and S. Du, Anti-Parity-Time Symmetric Optical Four-Wave Mixing in Cold Atoms, Phys. Rev. Lett. **123**, 193604 (2019).

[16] Y. Choi, C. Hahn, J. W. Yoon, and S. H. Song, Observation of an anti-PT-symmetric exceptional point and energy difference conserving dynamics in electrical circuit resonators, Nat. Commun. **9**, 2182 (2018).

[17] Y. Li, Y.-G. Peng, L. Han, M.-A. Miri, W. Li, M. Xiao, X.-F. Zhu, J. Zhao, A. Alù, S. Fan, and C.-W. Qiu, Anti-parity-time symmetry in diffusive systems, Science **364**, 170 (2019).

[18] J. Zhao, Y. L. Liu, L. H. Wu, C.-K. Duan, Y.-X. Liu, and J. F. Du, Observation of Anti-$\mathcal{PT}$-Symmetry Phase Transition in the

Magnon-Cavity-Magnon Coupled System, Phys. Rev. Appl. **13**, 014053 (2020).

[19] X.-L. Zhang, T. Jiang, and C. T. Chan, Dynamically encircling an exceptional point in anti-parity-time symmetric systems: Asymmetric mode switching for symmetry-broken modes, Light Sci. Appl. **8**, 1 (2019).

[20] H. Fan, J. Chen, Z. Zhao, J. M. Wen, and Y.-P. Huang, Antiparity-time symmetry in passive nanophotonics, ACS Photonics, **7**, 3035 (2020).

[21] F. X. Zhang, Y. M. Feng, X. F. Chen, L. Ge, and W. J. Wan, Synthetic Anti-PT Symmetry in a Single Microcavity, Phys. Rev. Lett. **124**, 053901 (2020).

[22] F. Yang, Y.-C. Liu, and L. You, Anti-PT symmetry in dissipatively coupled optical systems, Phys. Rev. A **96**, 053845 (2017).

[23] H. L. Zhang, R. Huang, S.-D. Zhang, Y. Li, C.-W. Qiu, F. Nori, and H. Jing, Breaking Anti-PT symmetry by spinning a resonator, Nano Lett. **20**, 7594 (2020).

[24] J. W. Wen, G. Q. Qin, C. Zheng, S. J. Wei, X. Y. Kong, T. Xin, and G. L. Long, Observation of information flow in the anti-$\mathcal{PT}$-symmetric system with nuclear spins, npj Quantum Inf. **6**, 28 (2020).

[25] J.-H. Wu, M. Artoni, and G. C. La Rocca, Non-Hermitian Degeneracies and Unidirectional Reflectionless Atomic Lattices, Phys. Rev. Lett. **113**, 123004 (2014).

[26] M. Aspelmeyer, T. J. Kippenberg, and F. Marquardt, Cavity optomechanics, Rev. Mod. Phys. **86**, 1391 (2014).

[27] H. Xiong, L. G. Si, X. Y. Lv, X. X. Yang, and Y. Wu, Review of cavity optomechanics in the weak-coupling regime: From linearization to intrinsic nonlinear interactions, Sci. China: Phys. Mech. Astron. **58**, 1 (2015).

[28] Y.-L. Liu, C. Wang, J. Zhang, and Y.-X. Liu, Cavity optomechanics: Manipulating photons and phonons towards the single-photon strong coupling, Chin. Phys. B **27**, 024204 (2018).

[29] J. Chan, T. P. M. Alegre, A. H. Safavi-Naeini, J. T. Hill, A. Krause, S. Gröblacher, M. Aspelmeyer, and O. Painter, Laser cooling of a nanomechanical oscillator into its quantum ground state, Nature (London) **478**, 89 (2011).

[30] J. D. Teufel, T. Donner, D. Li, J. W. Harlow, M. S. Allman, K. Cicak, A. J. Sirois, J. D. Whittaker, K. W. Lehnert, and R. W. Simmonds, Sideband cooling of micromechanical motion to the quantum ground state, Nature (London) **475**, 359 (2011).

[31] R. W. Peterson, T. P. Purdy, N. S. Kampel, R. W. Andrews, P.-L. Yu, K. W. Lehnert, and C. A. Regal, Laser Cooling of a Micromechanical Membrane to the Quantum Backaction Limit, Phys. Rev. Lett. **116**, 063601 (2016).

[32] J. B. Clark, F. Lecocq, R. W. Simmonds, J. Aumentado, and J. D. Teufel, Sideband cooling beyond the quantum backaction limit with squeezed light, Nature (London) **541**, 191 (2017).

[33] L. Qiu, I. Shomroni, P. Seidler, and T. J. Kippenberg, Laser Cooling of a Nanomechanical Oscillator to Its Zero-Point Energy, Phys. Rev. Lett. **124**, 173601 (2020).

[34] U. Delić, M. Reisenbauer, K. Dare, D. Grass, V. Vuletić, N. Kiesel, and M. Aspelmeyer, Cooling of a levitated nanoparticle to the motional quantum ground state, Science **367**, 892 (2020).

[35] S. Weis, R. Rivière, S. Deléglise, E. Gavartin, O. Arcizet, A. Schliesser, and T. J. Kippenberg, Optomechanically induced transparency, Science **330**, 1520 (2010).

[36] A. H. Safavi-Naeini, T. P. Mayer Alegre, J. Chan, M. Eichenfield, M. Winger, Q. Lin, J. T. Hill, D. E. Chang, and O. Painter, Electromagnetically induced transparency and slow light with optomechanics, Nature (London) **472**, 69 (2011).

[37] E. E. Wollman, C. U. Lei, A. J. Weinstein, J. Suh, A. Kronwald, F. Marquardt, A. A. Clerk, and K. C. Schwab, Quantum squeezing of motion in a mechanical resonator, Science **349**, 952 (2015).

[38] J.-M. Pirkkalainen, E. Damskägg, M. Brandt, F. Massel, and M. A. Sillanpää, Squeezing of Quantum Noise of Motion in a Micromechanical Resonator, Phys. Rev. Lett. **115**, 243601 (2015).

[39] W. H. P. Nielsen, Y. Tsaturyan, C. B. Møller, E. S. Polzik, and A. Schliesser, Multimode optomechanical system in the quantum regime, Proc. Natl. Acad. Sci. USA **114**, 62 (2017).

[40] A. B. Shkarin, N. E. Flowers-Jacobs, S. W. Hoch, A. D. Kashkanova, C. Deutsch, J. Reichel, and J. G. E. Harris, Optically Mediated Hybridization between Two Mechanical Modes, Phys. Rev. Lett. **112**, 013602 (2014).

[41] M. Zhang, G. S. Wiederhecker, S. Manipatruni, A. Barnard, P. McEuen, and M. Lipson, Synchronization of Micromechanical Oscillators Using Light, Phys. Rev. Lett. **109**, 233906 (2012).

[42] W. L. Li, P. Piergentili, J. Li, S. Zippilli, R. Natali, N. Malossi, G. D. Giuseppe, and D. Vitali, Noise robustness of synchronization of two nanomechanical resonators coupled to the same cavity field, Phys. Rev. A **101**, 013802 (2020).

[43] R. Riedinger, A. Wallucks, I. Marinković, C. Löschnauer, M. Aspelmeyer, S. K. Hong, and S. Gröblacher, Remote quantum entanglement between two micromechanical oscillators, Nature (London) **556**, 473 (2018).

[44] C. F. Ockeloen-Korppi, E. Damskägg, J.-M. Pirkkalainen, M. Asjad, A. A. Clerk, F. Massel, M. J. Woolley, and M. A. Sillanpää, Stabilized entanglement of massive mechanical oscillators, Nature (London) **556**, 478 (2018).

[45] F. Massel, S. U. Cho, J.-M. Pirkkalainen, P. J. Hakonen, T. T. Heikkilä, and M. A. Sillanpää, Multimode circuit optomechanics near the quantum limit, Nat. Commun. **3**, 987 (2012).

[46] C. Jiang, Y. S. Cui, X. T. Bian, X. W. Li, and and G. B. Chen, Control of microwave signals using bichromatic electromechanically induced transparency in multimode circuit electromechanical systems, Chin. Phys. B **25**, 054204 (2016).

[47] C. F. Ockeloen-Korppi, M. F. Gely, E. Damskägg, M. Jenkins, G. A. Steele, and M. A. Sillanpää, Sideband cooling of nearly degenerate micromechanical oscillators in a multimode optomechanical system, Phys. Rev. A **99**, 023826 (2019).

[48] H. Xu, D. Mason, L. Y. Jiang, and J. G. E. Harris, Topological energy transfer in an optomechanical system with exceptional points, Nature (London) **537**, 80 (2016).

[49] A. Noguchi, R. Yamazaki, M. Ataka, H. Fujita, Y. Tabuchi, T. Ishikawa, K. Usami, and Y. Nakamura, Ground state cooling of a quantum electromechanical system with a silicon nitride membrane in a 3D loop-gap cavity, New J. Phys. **18**, 103036 (2016).

[50] H. Xu, L. Y. Jiang, A. A. Clerk, and J. G. E. Harris, Nonreciprocal control and cooling of phonon modes in an optomechanical system, Nature (London) **568**, 65 (2019).

[51] J. P. Mathew, J. Pino, and E. Verhagen, Synthetic gauge fields for phonon transport in a nano-optomechanical system, Nat. Nanotechnol. **15**, 198 (2020).

[52] A. Xuereb, C. Genes, and A. Dantan, Strong Coupling and Long-Range Collective Interactions in Optomechanical Arrays, Phys. Rev. Lett. **109**, 223601 (2012).

[53] L. F. Buchmann and D. M. Stamper-Kurn, Nondegenerate multimode optomechanics, Phys. Rev. A **92**, 013851 (2015).
[54] N. Spethmann, J. Kohler, S. Schreppler, L. Buchmann, and D. M. Stamper-Kurn, Cavity-mediated coupling of mechanical oscillators limited by quantum backaction, Nat. Phys. **12**, 27 (2016).
[55] P. Piergentili, L. Catalini, M. Bawaj, S. Zippilli, N. Malossi, R. Natali, D. Vitali, and G. D. Giuseppe, Two-membrane cavity optomechanics, New J. Phys. **20**, 083024 (2018).
[56] C. Gärtner, J. P. Moura, W. Haaxman, R. A. Norte, and S. Gröblacher, Integrated optomechanical arrays of two high reflectivity SiN membranes, Nano Lett. **18**, 7171 (2018).
[57] X. Wei, J. Sheng, C. Yang, Y. Wu, and H. Wu, Controllable two-membrane-in-the-middle cavity optomechanical system, Phys. Rev. A **99**, 023851 (2019).
[58] C. Yang, X. Wei, J. Sheng, and H. Wu, Phonon heat transport in cavity-mediated optomechanical nanoresonators, Nat. Commun. **11**, 4656 (2020).
[59] D.-G. Lai, J.-F. Huang, X.-L. Yin, B.-P. Hou, W. L. Li, D. Vitali, F. Nori, and J.-Q. Liao, Nonreciprocal ground-state cooling of multiple mechanical resonators, Phys. Rev. A **102**, 011502(R) (2020).
[60] J. Kohler, J. A. Gerber, E. Deist, and D. M. Stamper-Kurn, Simultaneous retrodiction of multimode optomechanical systems using matched filters, Phys. Rev. A **101**, 023804 (2020).
[61] J. Sheng, X. Wei, C. Yang, and H. Wu, Self-Organized Synchronization of Phonon Lasers, Phys. Rev. Lett. **124**, 053604 (2020).
[62] M. J. Weaver, F. Buters, F. Luna, H. Eerkens, K. Heeck, S. D. Man, and D. Bouwmeester, Coherent optomechanical state transfer between disparate mechanical resonators, Nat. Commun. **8**, 824 (2017).
[63] V. Fedoseev, F. Luna, W. Löffler, and D. Bouwmeester, Stimulated Raman Adiabatic Passage in Optomechanics, Phys. Rev. Lett. **126**, 113601 (2021).
[64] M. C. Kuzyk and H. Wang, Controlling multimode optomechanical interactions via interference, Phys. Rev. A **96**, 023860 (2017).
[65] K. R. Brown, C. Ospelkaus, Y. Colombe, A. C. Wilson, D. Leibfried, and D. J. Wineland, Coupled quantized mechanical oscillators, Nature (London) **471**, 196 (2011).
[66] P.-C. Ma, J.-Q. Zhang, Y. Xiao, M. Feng, and Z.-M. Zhang, Tunable double optomechanically induced transparency in an optomechanical system, Phys. Rev. A **90**, 043825 (2014).
[67] X. Y. Zhang, Y. H. Zhou, Y. Q. Guo, and X. X. Yi, Simultaneous cooling of two mechanical oscillators in dissipatively coupled optomechanical systems, Phys. Rev. A **100**, 023807 (2019).
[68] H. Okamoto, A. Gourgout, C.-Y. Chang, K. Onomitsu, I. Mahboob, E. Y. Chang, and H. Yamaguchi, Coherent phonon manipulation in coupled mechanical resonators, Nat. Phys. **9**, 480 (2013).
[69] D.-G. Lai, X. Wang, W. Qin, B.-P. Hou, F. Nori, and J.-Q. Liao, Tunable optomechanically induced transparency by controlling the dark-mode effect, Phys. Rev. A **102**, 023707 (2020).
[70] X.-W. Xu, Y.-X. Liu, C.-P. Sun, and Y. Li, Mechanical $\mathcal{PT}$ symmetry in coupled optomechanical systems, Phys. Rev. A **92**, 013852 (2015).
[71] Y.-L. Liu and Y.-X. Liu, Energy-localization-enhanced ground-state cooling of a mechanical resonator from room temperature in optomechanics using a gain cavity, Phys. Rev. A **96**, 023812 (2017).
[72] H. Jing, Ş. K. Özdemir, H. Lü, and F. Nori, High-order exceptional points in optomechanics, Sci. Rep. **7**, 3386 (2017).
[73] N. R. Bernier, L. D. Toth, A. K. Feofanov, and T. J. Kippenberg, Level attraction in a microwave optomechanical circuit, Phys. Rev. A **98**, 023841 (2018).
[74] A. A. Clerk, M. H. Devoret, S. M. Girvin, F. Marquardt, and R. J. Schoelkopf, Introduction to quantum noise, measurement, and amplification, Rev. Mod. Phys. **82**, 1155 (2010).
[75] I. Wilson-Rae, N. Nooshi, W. Zwerger, and T. J. Kippenberg, Theory of Ground State Cooling of a Mechanical Oscillator Using Dynamical Backaction, Phys. Rev. Lett. **99**, 093901 (2007).
[76] F. Marquardt, J. P. Chen, A. A. Clerk, and S. M. Girvin, Quantum Theory of Cavity-Assisted Sideband Cooling of Mechanical Motion, Phys. Rev. Lett. **99**, 093902 (2007).
[77] Q. Zhong, M. Khajavikhan, D. N. Christodoulides, and R. El-Ganainy, Winding around non-Hermitian singularities, Nat. Commun. **9**, 4808 (2018).
[78] J. Doppler, A. A. Mailybaev, J. Böhm, U. Kuhl, A. Girschikm, F. Libisch, T. J. Milburn, P. Rabl, N. Moiseyev, and S. Rotter, Dynamically encircling an exceptional point for asymmetric mode switching, Nature (London) **537**, 76 (2016).